ChemComm

COMMUNICATION

View Article Online
View Journal | View Issue

Cite this: *Chem. Commun.*, 2025, **61**, 2119

Received 5th October 2024,
Accepted 16th December 2024

DOI: 10.1039/d4cc05227g

rsc.li/chemcomm

A two-dimensional amorphous iridium–cobalt oxide for an acidic oxygen evolution reaction†

Da Liu,[a] Yue Wang,[a] Jiarui Zhu,[b] Xuewei Gu,[b] Hao Yang, *[b] Yutian Xiong,[a] Mingwang Shao *[b] and Qi Shao *[a]

A two-dimensional (2D) amorphous iridium cobalt oxide (Am-$IrCo_yO_x$) was prepared using the molten salt method. The optimal catalyst shows a low overpotential of 230 mV at 10 mA cm^{-2} in 0.5 M H_2SO_4. DFT calculations show that the unsaturated Ir active sites on the surface are responsible for the excellent electrocatalytic performance. This work exhibits the advantages of 2D oxides and might find potential applications in other fields.

Hydrogen (H_2) is considered a clean energy source due to its high energy density and zero carbon emissions.[1] Consequently, the electrochemical water splitting reaction that can generate hydrogen has received great attention and can be conducted in acidic, neutral, or alkaline media.[2] However, the anodic oxygen evolution reaction (OER) is a four-electron transfer process with slow reaction kinetics and high energy barriers, which results in poor performance of the OER. Therefore, it remains a challenge to design efficient OER catalysts.[3]

Compared to alkaline or neutral electrolytes, the use of acidic conditions offers advantages such as low ohmic losses and a high current density.[4] Membrane-free electrolysis may be one solution,[5,6] yet limited by the lack of appropriate acid stable catalysts. Thus developing new acid stable OER catalysts is urgent.[7] Iridium oxide (IrO_2) is considered the benchmark catalyst for the acidic OER.[8] However, the scarcity and cost of iridium (Ir) limit its wide application.[9] Introducing a non-noble metal into IrO_2 can be an effective strategy to solve this problem.[10] Non-noble metals with 3d orbitals have received significant consideration because their orbitals can interact with the orbitals of 5d noble metals, resulting in versatile electronic structures for the OER activity.[11] Among all 3D non-noble metals, cobalt (Co) has been widely utilized for activating the OER activity, as demonstrated by both experimental data and theoretical calculations.[12] Therefore, one available approach is to combine a small amount of the noble metal Ir with Co to form the iridium–cobalt oxide to obtain a low-cost, high-performance OER electrocatalyst.[13]

Recently, two-dimensional (2D) amorphous catalysts, due to their unique structure, exhibit higher atomic utilization, more defects, and dangling bonds, which endow them with special physical and chemical properties, thereby enhancing their catalytic performance.[14,15] Therefore, the development of a 2D amorphous iridium cobalt oxide will provide insights into achieving high OER performance.

In this work, we synthesised a 2D amorphous iridium cobalt oxide (Am-$IrCo_5O_x$), with an Ir/Co atomic ratio of 1 : 5, for acidic OER catalysts using a molten salt method. Am-$IrCo_5O_x$ shows a low overpotential of 230 mV at 10 mA cm^{-2} in 0.5 M H_2SO_4, which is lower than commercial iridium oxide (C-IrO_2) (300 mV). DFT calculations show that the unsaturated Ir active sites on the surface are responsible for achieving the low overpotential of the acidic OER. This study not only proposes a strategy for synthesizing binary metal oxides to reduce the cost of use but also provides a feasible method for the synthesis of 2D amorphous oxides.

We used a simple molten salt method approach to synthesize a 2D amorphous iridium cobalt oxide (Am-$IrCo_yO_x$, y is the atomic ratio of Co to Ir) (Fig. 1a). The scanning electron microscope (SEM) and transmission electron microscope (TEM) images indicate that Am-$IrCo_5O_x$ exhibits a nanosheet morphology (Fig. 1d and e). The AFM image indicates that the thickness of Am-$IrCo_5O_x$ is approximately 1.26 nm (Fig. 1c). In X-ray diffraction (XRD), Am-$IrCo_5O_x$ does not exhibit distinct characteristic peaks, indicating its amorphous nature (Fig. 1b). Meanwhile, in the high-resolution transmission electron microscopy (HRTEM) image, the absence of distinct crystal morphology indicates that Am-$IrCo_5O_x$ possesses an amorphous structure (Fig. 1f). Besides, from the selected area electron diffraction (SAED) image (Fig. 1g), it can be found that Am-$IrCo_5O_x$ presents no obvious bright spots

[a] College of Chemistry, Chemical Engineering and Materials Science, Soochow University, 215123 Jiangsu, China. E-mail: qshao@suda.edu.cn
[b] Institute of Functional Nano & Soft Materials (FUNSOM), Jiangsu Key Laboratory for Carbon-Based Functional Materials & Devices, Soochow University, 199 Ren'ai Road, Suzhou, 215123, Jiangsu, China. E-mail: haoyang@suda.edu.cn, mwshao@suda.edu.cn

† Electronic supplementary information (ESI) available. See DOI: https://doi.org/10.1039/d4cc05227g

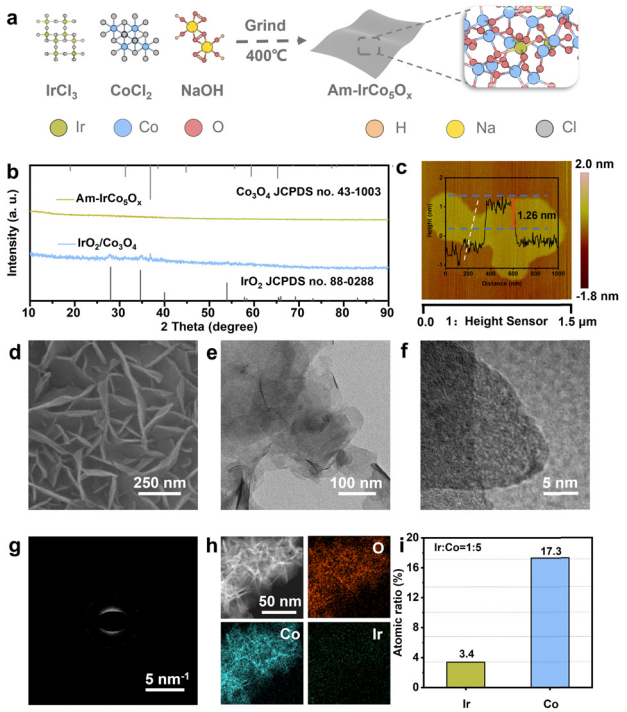

Fig. 1 (a) Schematic illustration for the synthesis process. (b) XRD patterns of Am-$IrCo_5O_x$, Am-$IrCo_6O_x$ and Am-$IrCo_4O_x$. (c) AFM image of Am-$IrCo_5O_x$. (d) SEM image of Am-$IrCo_5O_x$. (e) TEM image of Am-$IrCo_5O_x$. (f) HRTEM image of Am-$IrCo_5O_x$. (g) SAED pattern of Am-$IrCo_5O_x$. (h) STEM-EDS elemental mapping images of Am-$IrCo_5O_x$. (i) Atomic ratio of Ir and Co.

and clear rings, also manifesting the amorphousness of Am-$IrCo_5O_x$. Elemental mapping images also show homogeneous dispersion of Ir, Co, and O atoms throughout the entire Am-$IrCo_5O_x$ sample (Fig. 1h).

By controlling the amounts of $IrCl_3$ and $CoCl_2{\cdot}6H_2O$ reactants, various iridium–cobalt oxides can be obtained. At ratios of 1 : 6 and 1 : 7 for $IrCl_3$ to $CoCl_2{\cdot}6H_2O$, as observed *via* SEM and TEM, the morphologies persist as nanosheets (Fig. S7a, b and S8a and b, ESI†). However, at ratios of 1 : 3 and 1 : 4 for $IrCl_3$ to $CoCl_2{\cdot}6H_2O$, as observed, the morphology of nanoparticles appeared (Fig. S5a, b and S6a, b, ESI†). XRD shows that Am-$IrCo_3O_x$, Am-$IrCo_4O_x$, Am-$IrCo_6O_x$ and Am-$IrCo_7O_x$ are amorphous (Fig. S5d, S6d, S7d and S8d, ESI†). Elemental mapping images demonstrate the uniform distribution of Ir, Co, and O atoms in Am-$IrCo_3O_x$, Am-$IrCo_4O_x$, Am-$IrCo_6O_x$ and Am-$IrCo_7O_x$ (Fig. S5c, S6c, S7c and S8c, ESI†). This indicates that the introduction of excess Ir will affect the morphology of the amorphous nanosheets, resulting in the formation of amorphous nanoparticles.

To understand the electronic structure of Am-$IrCo_5O_x$, we carried out X-ray photoelectron spectroscopy (XPS). The survey XPS spectra of Am-$IrCo_5O_x$ demonstrate the existence of Ir, Co and O elements (Fig. 2a). As shown in Fig. 2b, Ir XPS in IrO_2/Co_3O_4 shows a set of double peaks at 61.9 eV and 64.9 eV, which can be attributed to Ir^{4+}. For Am-$IrCo_5O_x$, the Ir 4f spectrum can be deconvoluted into two sets of doublets centered at 61.7/64.9 eV

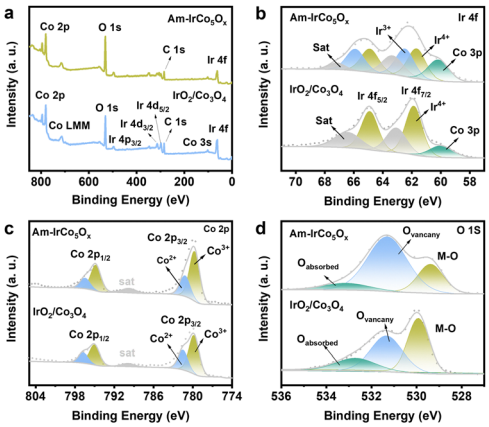

Fig. 2 (a) The full range XPS spectra of Am-$IrCo_5O_x$ and IrO_2/Co_3O_4. (b) Ir 4f XPS spectra of Am-$IrCo_5O_x$ and IrO_2/Co_3O_4. (c) Co 2p XPS spectra of Am-$IrCo_5O_x$ and IrO_2/Co_3O_4. (d) O 1s XPS spectra of Am-$IrCo_5O_x$ and IrO_2/Co_3O_4.

and 62.5/65.9 eV, which can be attributed to Ir^{4+} and Ir^{3+}, respectively.[16] The peak located at 60.6 eV is produced by Co 3p. The introduction of Ir affects the electronic structure of cobalt oxide; as revealed in Fig. 2c, the main peaks of Co 2p3/2 of both Am-$IrCo_5O_x$ and the as-synthesized IrO_2/Co_3O_4 present signals that can be identified as Co^{2+} and Co^{3+}, respectively. Nevertheless, the Co^{2+} over Co^{3+} ratio is decreased by 12.5% after Ir species are introduced (the ratios of Co^{2+} : Co^{3+} in IrO_2/Co_3O_4 and Am–$IrCo_5O_x$ are 0.48 : 1 and 0.42 : 1, respectively). According to Fig. 2d, the Am-$IrCo_5O_x$ sample has more oxygen vacancies. Also the EPR spectral signals show that at g = 2.002, the signal of Am-$IrCo_5O_x$ is stronger than that of IrO_2/Co_3O_4 (Fig. S9, ESI†).

The OER performance of Am-$IrCo_5O_x$ and the prepared IrO_2/Co_3O_4 in 0.5 M H_2SO_4 was studied in a standard three-electrode system and compared with that of C-IrO_2. All measured potentials calibrated to the reversible hydrogen electrode (RHE) (Fig. S10, ESI†). In terms of reaching the current density of 10 mA cm^{-2}, Am-$IrCo_5O_x$ requires an overpotential (η) of 230 mV, which is lower than those of IrO_2/Co_3O_4 (322 mV) and C-IrO_2 (300 mV) (Fig. 3a and b). Then multiple experiments were conducted to demonstrate the reproducibility of the results (Fig. 3b and Fig. S11, ESI†). In addition, the outstanding OER activity of Am-$IrCo_5O_x$ is also reflected by a superior Tafel slope of 61.5 mV dec^{-1} compared to that of IrO_2/Co_3O_4 (66.7 mV dec^{-1}) and that of C-IrO_2 (64.3 mV dec^{-1}), indicating that the OER kinetics of Am-$IrCo_5O_x$ is significantly accelerated (Fig. 3c). The C_{dl} values of these catalysts were obtained by cyclic voltammetry (Fig. S12 and S13, ESI†).

To further explain the high catalytic activity, electrochemical impedance spectroscopy (EIS) measurements of these three samples were tested under the same conditions, as shown in Fig. S14 (ESI†). The Nyquist diagram shows that among the tested catalysts, Am-$IrCo_5O_x$ exhibits the lowest charge transfer resistance, confirming its highest catalytic activity. The fastest charge transfer rate of Am-$IrCo_5O_x$ may be attributed to its ultra-thin nanosheet structure and abundant oxygen vacancies.

Next, the intrinsic activity of various catalysts in the OER was evaluated by mass activity evaluation.[17,18] Am-$IrCo_5O_x$ shows a

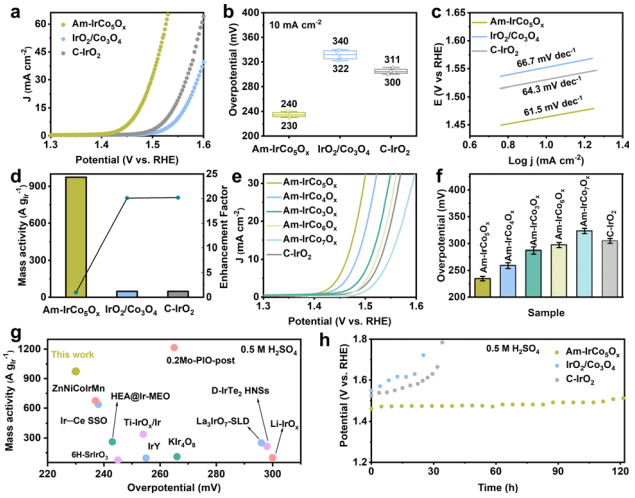

Fig. 3 (a) Polarization curves of Am-$IrCo_5O_x$, IrO_2/Co_3O_4 and C-IrO_2 in 0.5 M H_2SO_4 at a scanning rate of 5 mV s^{-1}. (b) Overpotential statistics at 10 mA cm^{-2} current density. (c) Tafel plots obtained from the polarization curves in (a). (d) Comparison of the mass activities of Am-$IrCo_5O_x$, IrO_2/Co_3O_4 and C-IrO_2 at 1.53 V *vs.* RHE. (e) Polarization curves of catalysts with different ratios of Ir and Co. (f) Comparison of the overpotential of catalysts with different ratios of Ir and Co at 10 mA cm^{-2}. (g) Comparison of the overpotential with other Ir-based catalysts. (h) Chronopotentiometry test of Am-$IrCo_5O_x$, IrO_2/Co_3O_4 and C-IrO_2 at a current density of 10 mA cm^{-2}.

high mass activity of 973.71 A g_{Ir}^{-1} at 1.53 V *vs.* RHE which is approximately 20.09 and 20.19 times higher than those of IrO_2/Co_3O_4 and C-IrO_2, respectively (Fig. 3d). A synopsis of previous literature is shown in Fig. 3g, highlighting the merits of Am-$IrCo_5O_x$ including its low overpotential and high mass activity, and Am-$IrCo_5O_x$ is found to be superior to most reported various Ir-based electrocatalysts (Table S1, ESI†).

In addition to the activity, durability is another crucial criterion for the electrocatalytic performance of catalysts towards the OER under operating conditions. As plotted in Fig. 3h, Am-$IrCo_5O_x$ shows long-term stability with a current density of 10 mA cm^{-2} for almost 122 h, which is superior to that of IrO_2/Co_3O_4 and C-IrO_2 catalysts. According to the SEM and TEM images shown in Fig. S15 (ESI†), the morphology of Am-$IrCo_5O_x$ has not changed significantly and has remained amorphous. Additionally, Inductively Coupled Plasma Mass Spectrometry (ICP-MS) was performed to determine the concentrations of dissolved Ir and Co in Am-$IrCo_5O_x$ after long-term stability testing under a constant current of 10 mA cm^{-2}. It can be found that the concentration of Ir and Co ions dissolved in the electrolyte during the 122 hour stability test of Am-$IrCo_5O_x$ is low (Table S2, ESI†), which proves that Am-$IrCo_5O_x$ has good stability. Although Am-$IrCo_5O_x$ exhibits good stability, during stability testing, a slight increase in overpotential and a decrease in activity inevitably occur, which is primarily attributed to the deactivation. When the catalyst was tested at 10 mA cm^{-2} for 122 h, the dissolved Ir and Co were 0.58 and 2.76 μg mL^{-1} (Table S2, ESI†), with about 0.06% Ir and 0.2% Co of the catalyst being dissolved. Thus, the main reason for deactivation is the dissolution of Co from the catalysts. In addition, the stability of Am-$IrCo_5O_x$, IrO_2/Co_3O_4, and IrO_2 was further tested at a high current density of 50 mA cm^2. As shown in Fig. S16 (ESI†), Am-$IrCo_5O_x$ exhibited long-term stability for 41 hours, significantly outperforming IrO_2/Co_3O_4 and C-IrO_2. This indicates that, under a high current density, Am-$IrCo_5O_x$ maintains excellent activity over an extended period. To investigate the differences in OER performance among different catalysts with varying Ir–Co atomic ratios, we performed Linear Sweep Voltammetry (LSV) of the catalysts (Fig. 3e). Am-$IrCo_5O_x$ (with an Ir to Co atomic ratio of 1 : 5) exhibits the best OER performance among all studied samples. It requires an overpotential of 230 mV to achieve a current density of 10 mA cm^{-2}, which is lower compared to those of Am-$IrCo_4O_x$ (253 mV), Am-$IrCo_3O_x$ (280 mV), Am-$IrCo_6O_x$ (292 mV), and Am-$IrCo_7O_x$ (317 mV), as listed in Table S3 (ESI†). The C_{dl} values of Am-$IrCo_yO_x$ catalysts were obtained by cyclic voltammetry (Fig. S17 and S18, ESI†).

The IR spectroscopy results provide information about phase composition and the bonding modes of oxygen with metal ions. The IR transmission spectrum of Am-$IrCo_5O_x$ powder is shown in Fig. S20a (ESI†). The infrared spectrum of IrO_2/Co_3O_4 consists of two infrared transmission bands at 580 cm^{-1} and 670 cm^{-1}. In IrO_2/Co_3O_4, the absorption peak at 580 cm^{-1} is related to the Co–O vibrations at octahedral sites, while the peak at 670 cm^{-1} corresponds to the vibrations of Co–O at tetrahedral sites.[19] In Am-$IrCo_5O_x$, there exists only an octahedral Co–O vibration peak at 580 cm^{-1}. Existing experimental findings suggest that the redox-active octahedra are critical in oxygen electrocatalysis.[20] The redox-active transition metal located at the octahedral site guarantees an effective interaction with oxygen under OER conditions. Furthermore, adjacent octahedral centres act synergistically to promote fast OER kinetics. In contrast, isolated tetrahedral centres in spinel cobalt oxide suppresses the OER mediated by octahedral centre sites.[20,21] The IR transmission spectra of Am-$IrCo_3O_x$, Am-$IrCo_4O_x$, Am-$IrCo_6O_x$ and Am-$IrCo_7O_x$ powder in the wavelength range of 400–1000 cm^{-1} are shown in Fig. S20b (ESI†). The intensity of the Co–O vibration peak at the octahedral sites in Am-$IrCo_5O_x$ is higher than that in Am-$IrCo_3O_x$, Am-$IrCo_4O_x$, Am-$IrCo_6O_x$ and Am-$IrCo_7O_x$. This indicates that when the Ir-to-Co ratio is 1 : 5, the octahedral Co–O configuration is most abundant in Am-$IrCo_yO_x$.

Fig. S21 (ESI†) shows the Raman spectra of Am-$IrCo_5O_x$, Co_3O_4, and IrO_2. The Am-$IrCo_5O_x$ electrode displayed seven distinct peaks at 379 cm^{-1}, 416 cm^{-1}, 484 cm^{-1}, 524 cm^{-1}, 570 cm^{-1}, 679 cm^{-1} and 740 cm^{-1}. The α peak represents the characteristic vibrational mode of Co–O octahedral coordination in the Co_3O_4 crystal structure, while the μ peak represents the characteristic vibrational mode of Co–O tetrahedral coordination in the Co_3O_4 crystal structure.[22] In Am-$IrCo_5O_x$, there exists only an octahedral Co–O vibration peak at the α peak. This is consistent with the results of IR spectroscopy. Meanwhile, the Raman spectrum of Am-$IrCo_5O_x$ exhibited Ir–O vibrational peaks, namely the ε, δ, η, and λ peaks.

Density functional theory (DFT) calculations were employed to explore the real sites as well as the dominant mechanism of the OER occurring on amorphous iridium cobalt oxides. To mimic the experimentally observed amorphous structure, we adopted the Monte Carlo annealing strategy to construct the relatively low coordinated Am-$IrCo_5O_x$ (see more details in the ESI†).

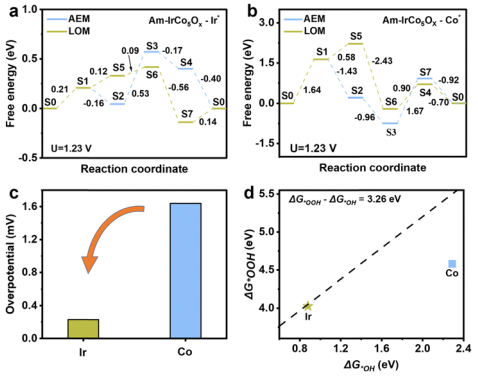

Fig. 4 Gibbs free energy diagrams of (a) Ir sites and (b) Co sites on the Am-$IrCo_5O_x$ surface under a bias potential of 1.23 V *vs.* RHE. (c) Comparison of the calculated overpotentials for Ir and Co sites on Am-$IrCo_5O_x$. (d) The binding energies of *OOH *vs.* *OH for Ir and Co sites on Am-$IrCo_5O_x$. The dashed line represents a linear scaling relationship between the *OH and *OOH intermediates for the optimal OER catalysts.

Typically, as the key elementary step of O–O bond formation during the OER, two distinctive mechanisms, *i.e.* the adsorbate evolution mechanism (AEM) and the lattice oxygen mechanism (LOM), have been proposed.[23,24] The main difference between these two mechanisms is the oxygen source participating in the whole reaction. It is much more intriguing to understand the dominant mechanism of Am-$IrCo_5O_x$ since there are many more under-coordinated metal sites that exist on the surface derived from low crystallinity. The optimized structures of all states for the OER on Am-$IrCo_5O_x$ are shown in Fig. S22 and S23 (ESI†). As shown in Fig. 4a, b and Fig. S24 (ESI†), both AEM and LOM pathways were simulated on Ir or Co sites on the Am-$IrCo_5O_x$ surface, with the results listed in Table S4 and S5 (ESI†). It can be seen that the OER followed by the LOM easily occurs due to its relatively low overpotential than the AEM, either on Ir or Co sites. Additionally, the Ir sites in Am-$IrCo_5O_x$ can achieve the 230 mV overpotential required for the LOM pathway, which is significantly lower than that at the Co sites, in agreement with experimental values (Fig. 4c). Moreover, the binding difference between *OOH and *OH at the Ir sites is closer to the optimal value than that at the Co sites (Fig. 4d).[25] Therefore, it can be concluded that the Ir sites on Am-$IrCo_5O_x$ are more active than the Co sites.

In summary, a 2D amorphous iridium cobalt oxide was successfully prepared *via* molten salt synthesis. Irregular atomic variations in Am-$IrCo_5O_x$ lead to increased oxygen vacancies and the presence of low-valence iridium, contributing to its exceptional acidic OER performance. At a current density of 10 mA cm^{-2}, Am-$IrCo_5O_x$ exhibits a low overpotential of only 230 mV. IR spectroscopy shows that Am-$IrCo_5O_x$ has only an octahedral configuration, which ensures efficient interaction of the catalyst with oxygen and promotes fast OER kinetics. Thus, we have successfully developed this two-dimensional amorphous oxide, providing a new pathway to reduce the usage of noble metals.

Data availability

The data supporting this article have been included as part of the ESI.†

Conflicts of interest

There are no conflicts to declare.

Notes and references

1 X. Li, *et al.*, *Nat. Commun.*, 2021, **12**, 2351.
2 S. Chu and A. Majumdar, *Nature*, 2012, **488**, 294–303.
3 L. C. Seitz, *et al.*, *Science*, 2016, **353**, 1011–1014.
4 S. Hu, *et al.*, *Adv. Funct. Mater.*, 2022, **32**, 2201726.
5 M. Iesalnieks, *et al.*, *Adv. Sci.*, 2024, **11**, 2401261.
6 M. Vanags, *et al.*, *Int. J. Hydrogen Energy*, 2023, **48**, 20551–20561.
7 P. C. Sherrell, *et al.*, *Adv. Energy Sustainability Res.*, 2024, **5**, 2400008.
8 C. C. L. McCrory, *et al.*, *J. Am. Chem. Soc.*, 2013, **135**, 16977–16987.
9 J. Shan, *et al.*, *Chem*, 2019, **5**, 445–459.
10 X. Liu, *et al.*, *Nat. Commun.*, 2021, **12**, 5676.
11 L. Li, *et al.*, *Adv. Funct. Mater.*, 2021, **31**, 2104746.
12 X. Yuan, *et al.*, *ACS Energy Lett.*, 2017, **2**, 1208–1213.
13 J. Song, *et al.*, *Chem. Soc. Rev.*, 2020, **49**, 2196–2214.
14 X. Kong, *et al.*, *SmartMat*, 2023, **4**, e1152.
15 J. Khan, *et al.*, *SmartMat*, 2023, **4**, e1156.
16 V. Pfeifer, *et al.*, *Phys. Chem. Chem. Phys.*, 2016, **18**, 2292–2296.
17 J. Li, *et al.*, *ChemSusChem*, 2024, **17**, e202400239.
18 G. T. K. K. Gunasooriya and J. Nørskov, *ACS Energy Lett.*, 2020, **5**, 3778–3787.
19 M. Mayakannan, *et al.*, *Mater. Chem. Phys*, 2020, **242**, 122282.
20 Y. Zhou, *et al.*, *Adv. Mater.*, 2019, **31**, 1902509.
21 W. Zhu, *et al.*, *J. Am. Chem. Soc.*, 2023, **145**, 17995–18006.
22 R. Zhang, *et al.*, *J. Am. Chem. Soc.*, 2023, **145**, 2271–2281.
23 I. C. Man, *et al.*, *ChemCatChem*, 2011, **3**, 1159–1165.
24 F. Dionigi, *et al.*, *Nat. Commun.*, 2020, **11**, 2522.
25 M. J. Craig, *et al.*, *Nat. Commun.*, 2019, **10**, 4993.

